Single-Fluorophore Detection in Femtoliter Droplets Generated by Flow Focusing

Robert Weinmeister,[†,‡] Emma Freeman,[‡] Ian C. Eperon,[†] Alison M. Stuart,[‡] and Andrew J. Hudson[*,‡]

[†]Department of Biochemistry, University of Leicester, Leicester, LE1 9HN, United Kingdom and [‡]Department of Chemistry, University of Leicester, Leicester, LE1 7RH, United Kingdom

ABSTRACT Aqueous microdroplets with a volume of a few femtoliters are an ideal sample size for single-molecule fluorescence experiments. In particular, they enable prolonged measurements to be made on individual molecules that can diffuse freely in the surrounding medium. However, the rapid production of monodisperse droplets in a hydrodynamic flow, such as microfluidic flow focusing, will often involve volumes that are typically too large (>0.5 pL) for single-molecule studies. Desired volumes of a few femtoliters, or smaller, can be produced by either tip streaming or step emulsification in a flow-focusing device; however, in both of these methods, the aqueous droplets are dispersed in a large volume of the continuous phase, where individual droplets can diffuse perpendicular to the flow direction, and the monodispersity of droplet size produced by tip streaming is difficult to sustain for more than transient time scales. We show here that the optimized design and fabrication of microfluidic devices with shallow channel depths can result in the reliable production of stable droplets of a few femtoliters at a high rate in the dripping regime of flow focusing. Furthermore, the generated microdroplets are localized in a two-dimensional plane to enable immediate analysis. We have demonstrated the fluorescence monitoring of single molecules of encapsulated green fluorescent protein. The apparatus is straightfoward, inexpensive, and readily assembled within an ordinary laboratory environment.

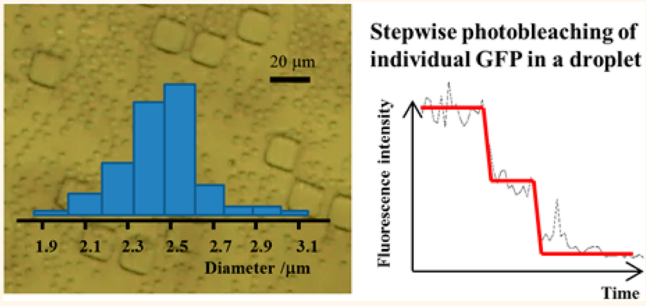

KEYWORDS: single-molecule fluorescence · digital microfluidics · flow focusing · lab-on-a-chip · soft lithography · droplet encapsulation · *in vitro* compartmentalization

Single-molecule experiments have become an extremely important tool for the investigation of biological reactions. One of the most common uses is in fluorescence imaging, where measurements of fluorescence resonance energy transfer (FRET) have contributed much to our understanding of macromolecular dynamics and reaction pathways. A particular problem arises, however, with complex reactions that can take a long time *in vitro*. A good example is in studies of pre-mRNA splicing, where the reaction can be supported only in crude extracts and may take hours. Single-molecule studies of splicing have been possible using total internal reflection fluorescence (TIRF) microscopy.[1,2] In these experiments, one component (typically the pre-mRNA substrate) is attached to the surface of a glass or silica coverslip, but this procedure suffers from the possibility that tethering will affect the kinetics of association of large macromolecular complexes. In addition, if freely diffusing components of the reaction are labeled also, they may adsorb to the surface and obscure events on the target site. This problem has been encountered with proteins that regulate mammalian splicing reactions, because they have to be present at relatively high concentrations to function and readily adsorb to surfaces.[1,2] An alternative strategy is to detect FRET or interactions in freely diffusing molecules as they pass through a confocal laser (for example, by fluorescence correlation spectroscopy or alternating laser excitation spectroscopy), but this precludes following the sequence of events in a single molecule (or complex) over a period of time.

A promising method for following the reactions of single molecules for a prolonged time without tethering them is to

* Address correspondence to andrew.hudson@leicester.ac.uk.

Received for review April 22, 2015 and accepted September 12, 2015.

Published online September 13, 2015
10.1021/acsnano.5b02422

encapsulate them into emulsion droplets. The isolated molecules can then be imaged and analyzed individually by confocal observation of a single droplet, or a larger number of droplets can be imaged concurrently in a wide-field mode, using a highly inclined thin illumination laser beam[3] or TIRF microscopy. Indeed, it would be more desirable to image droplets in a wide-field mode. For both inclined and TIRF illumination geometries, the emulsion droplets would need to be small (approximately 1 μm length in the axial dimension) and positioned directly above the imaging surface; although the intensity of the evanescent field used in TIRF microscopy falls significantly beyond distances of 50−100 nm from the surface, the excitation light can still be coupled efficiently into aqueous droplets dispersed in a low-index perfluorocarbon oil. Droplets[4] or vesicles[5] used for studying biological reactions, including single-molecule studies, have for the most part been either relatively large in size (>10 μm, or >0.5 pL) or produced individually or have necessitated imaging by confocal methods only. There has been relatively little success in forming droplets with volumes in the region of a few femtoliters.

Tawfik and Griffiths were the first to show the utility of water-in-oil emulsions for *in vitro* biology by compartmentalizing the transcription and translation of single genes within aqueous droplets of variable size (mean spherical diameter, 2−3 μm).[6] In these early experiments, the emulsion droplets were formed by stirring the aqueous reaction mixture with mineral oil and surfactant, and the products of gene expression were measured after breaking the emulsion to extract the aqueous phase. Goldner and co-workers demonstrated the *in situ* measurement of single fluorescent molecules within similar-sized droplets (hydrosomes) that were also formed by stirring aqueous and oil phases together.[7] In this example, the continuous phase of the emulsion was a perfluorocarbon oil with low refractive index, which meant that the aqueous droplets could be held by optical tweezers and a single encapsulated molecule could be monitored for a period of time by confocal fluorescence microscopy. The authors showed that two droplets could be fused together using a pair of independent optical traps, and, in subsequent work, they demonstrated a droplet-on-demand method for producing and mixing aqueous droplets of monodisperse size in optical traps (both femtoliter and subfemtoliter volume).[8] Although the combination of optical trapping and droplet-on-demand is an elegant methodology, it is a relatively slow procedure for gathering data sets on a large number of single molecules, which is essential for understanding the static and dynamic heterogeneity in single-molecule experiments. There is, therefore, a need for a method to produce emulsion droplets rapidly and with monodisperse-femtoliter size suitable for encapsulating individual molecules. This would address the main disadvantage of limited data sets obtained in experiments using either droplet-on-demand techniques or tethered lipid vesicles.

One approach to this is the use of small surface features that trigger droplet formation. This had been done, first, by partitioning an aqueous sample between approximately 10^5 micrometer-sized cavities (with individual volumes of 1.4 to 100 fL) in a silicone substrate[9] and then by using a surface containing an array of hydrophilic circular patterns (4.8 μm in diameter) isolated on a hydrophobic polymer nanolayer.[10] Sessile-type aqueous droplets form on each of the hydrophilic centers (with approximate volumes of 14.8 fL) by the exchange of an aqueous layer on the surface with oil; the contents of individual droplets can be changed by contact with a micropipette. Similar results were achieved[11] by exchanging the aqueous layer on the surface of a microcavity array with oil, which leaves the hydrophilic microcavities occupied with isolated aqueous volumes of 120 fL. The loading of microcavities of 38 fL volume with magnetic beads conjugated to single protein molecules enabled Lammertyn and co-workers[12] to add reagents sequentially by exchanging aqueous and oil phases in the presence of a magnetic field. Wu *et al.*[13] have demonstrated very small droplet arrays by filling an array of picoliter microcavities and then allowing the droplets to shrink to ~5 fL by controlled water diffusion to the continuous oil layer. However, the potential utility of all these methods as a tool for single-molecule *in vitro* biology is affected negatively by the initial exposure of imaging surfaces to a large volume of aqueous solution prior to sample compartmentalization and the aforementioned critical problem of adsorption of labeled molecules to exposed surfaces.

Flow focusing[14] involves rapid and continuous droplet production using coflowing streams of immiscible liquids. It has found wide applications in *in vitro* high-throughput biology,[15−20] but, as with the other microfluidic methods, it has not been used widely for encapsulation and detection of a single fluorophore. Flow focusing has been used predominantly for the controlled production of normal and reverse monodisperse emulsions over a wide range of large droplet sizes from 500 nL (1000 μm diameter) down to 4 pL (20 μm diameter).[21] The microfluidic method is passive and relies on an upstream flow field ahead of a four-way junction in which one liquid phase is sandwiched between immiscible liquid phases in coflowing streams (see Figure 1). The pressure in the upstream fluidic channels is not in equilibrium and subject to periodic oscillations that lead to competition between the aqueous and oil flow. In the example shown in Figure 1, a transient increase in the pressure of the aqueous phase limits the flow of the oil phases and a pendant-like droplet forms at the four-way junction.

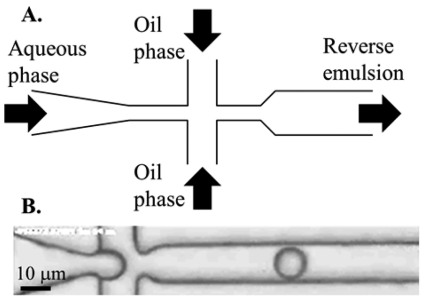

Figure 1. Microfluidic flow focusing. Aqueous and oil phases converge at a four-way junction, leading to the dispersion of the aqueous phase in the oil.

While the droplet size increases, the pressure of the oil flow at the four-way junction also increases until the aqueous droplet is pinched off. At this time, the flow of the oil phase dominates and temporarily blocks the aqueous phase. The pressure of the aqueous phase increases again, and the process continues *ad infinitum* to generate a downstream flow of aqueous droplets dispersed in an immiscible oil. A theoretical account of the droplet-formation process has been given.[22]

The size of droplets formed by flow focusing will normally be dependent on the dimensions of the four-way junction (see Figure 1). Until now, the design of microfluidic devices by soft lithography with uniform feature sizes on the order of a few micrometers has been a challenge. The formation of oil droplets of approximately 1 fL (1 μm diameter) has been described in a microfluidic component where the exit-channel dimension of the junction was reduced (to approximately 1 μm) following the swelling of a polydimethylsiloxane (PDMS) substrate after it had been left in contact with water;[14] however, the manufacture of microfluidic devices with uniform narrow dimensions by aging in a moist environment would be unreliable. The production of droplets on the scale of 1 fL by microfluidic flow focusing is possible using junction dimensions of 10 μm or larger. A narrow thread must be formed in an aqueous phase sandwiched between fast flowing oil phases. Breakup of the thread can occur by a process called tip streaming to generate small droplet sizes;[23] however, the flow conditions for microdroplet formation by tip streaming cannot be maintained for longer than transient time scales, and precise control of droplet size is highly challenging. Droplets with a diameter of 3 μm (14 fL volume) have been formed by mixing water and oil phases at a nanofluidic T-junction[24,25] produced by photolithographic etching in borosilicate glass. However, this method of fabricating fluidic devices is distinctly disadvantageous compared with soft lithography techniques where a reusable mold is made that can produce any number of replicas outside of a clean room facility. Yang *et al.*[26] have demonstrated the formation of subfemtoliter droplets in a soft lithography device by initially forming much larger droplets by microfluidic flow focusing and further splitting of the droplets into uneven volumes at a downstream T junction, but the majority of the sample material is wasted in this method.

Step emulsification offers a robust microfluidic approach to obtain femtoliter droplet sizes in microfluidic devices. In this technique, first demonstrated by Nakajima and co-workers,[27] the flow of the dispersed phase undergoes a step change between the confines of a micrometer-sized channel and a larger volume containing the continuous phase. In Couture *et al.*,[28] a step change in the height of a channel immediately downstream of the four-way microfluidic junction of a flow-focusing device has enabled water-in-oil-in-water droplets of 4 μm diameter (34 fL volume) to be formed. The same geometry has been used for the parallelized production of fine emulsion droplets[29] and, recently, for the production of reagent-loaded droplets, with sizes down to 20 fL, that could be collected from the microfluidic device and used to compartmentalize the polymerase chain reaction.[30] While the step emulsification geometry offers a strategy to obtain suitably sized droplets for single-molecule measurements, a disadvantage is that the femtoliter droplets must be dispersed in channels that have undergone a transition to a large height. This means that the droplets will not remain in close proximity to an imaging surface, and they can diffuse in a direction perpendicular to the flow. This same drawback affects droplets produced by T-junction splitting.[26] Although the collection of droplets from the microfluidic device and reinjection (as demonstrated for various operations[30]) into a separate imaging device remains a possibility, the immediate imaging and analysis of droplets would be a great advantage for single-molecule experiments for which the statistics are impacted critically by photobleaching and denaturing.

In this paper, we demonstrate that the technique of microfluidic flow focusing can be adapted for the rapid and controlled formation of an emulsion containing monodisperse aqueous droplets with a size of approximately 1 fL volume (or approximately 1 μm spherical diameter) by scaling down a microfluidic flow-focusing device made using soft lithographic methods. The resulting aqueous droplets are suitable for confining single fluorophores and can be imaged immediately following their dispersion in the oil phase by established single-molecule spectroscopic techniques, such as total-internal reflection fluorescence. In this work, single molecules of green fluorescent protein have been encapsulated in the droplets and detected.

RESULTS

Generation of Femtoliter Droplets by Microfluidic Flow Focusing. A template to produce replicas of a flow-focusing device was kindly provided by A. D. Griffiths.[31] Using these replicas, monodisperse droplets with sizes

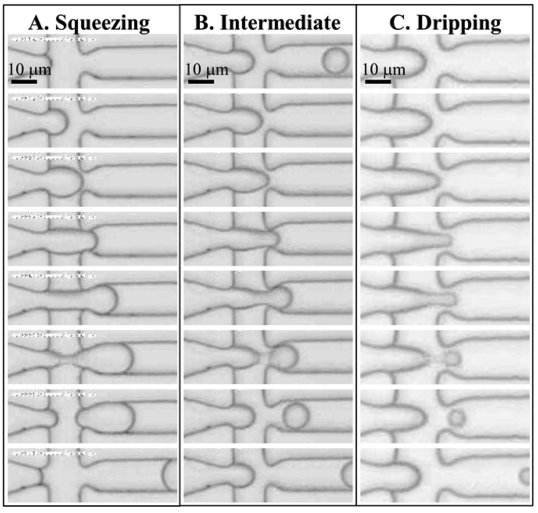

Figure 2. Droplet generation in replicas produced from the original template. (A) Squeezing regime. Image sequence recorded at 50 000 fps and 14 μs exposure time; frames shown at 0, 5.54, 6.78, 7.10, 7.46, 7.76, 7.78, and 9.12 ms. Aqueous flow rate 73 nL/min, oil flow rate 479 nL/min. (B) Intermediate regime. Images recorded at 57 601 fps and 14 μs exposure time; frames shown at 0, 0.57, 0.62, 0.68, 0.71, 0.73, 0.76, and 0.92 ms. Aqueous flow rate 59 nL/min, oil flow rate 899 nL/min. (C) Dripping regime. Images recorded at 52 002 fps and 12 μs exposure time; frames shown at 0, 12.31, 14.92, 15.23, 15.27, 15.29, 15.33, and 15.55 ms. Aqueous flow rate 5 nL/min, oil flow rate 965 nL/min.

down to around 500 fL (10 μm spherical diameter) could be generated continuously.

The contraction of the aqueous phase at the four-way junction in a flow-focusing device leads to an elongated flow, and the mode of breakup of the aqueous phase depends on the capillary number for the oil flow upstream of the junction. For small capillary numbers, the regime for droplet formation is called squeezing.[32,33] Under these conditions, the aqueous phase temporarily blocks the junction (see example in Figure 2A), and the flow of oil causes the pressure of the continuous phase to increase until a droplet is pinched off from the elongated aqueous flow. Increasing the pressure applied to the continuous phase reduces the formation time of the droplet, resulting in a decrease in size (Figure 2B) and increase in separation of droplets (see Figure 3A). The capillary number increases at higher flow rates of oil, and the mechanism for droplet formation transitions from squeezing into dripping (Figure 2C). In this case, the four-way junction is never blocked completely and, instead, the faster flow of oil causes the aqueous phase to deform into a focused flow. The droplets are pinched off from the end of the focused flow with diameters that can be equal to, or smaller than, the width of the junction. Using the original template, the smallest droplet sizes of 500 fL (10 μm diameter) were produced continuously by the dripping mechanism (shown in Figures 2C and 3A). It was possible to generate droplet

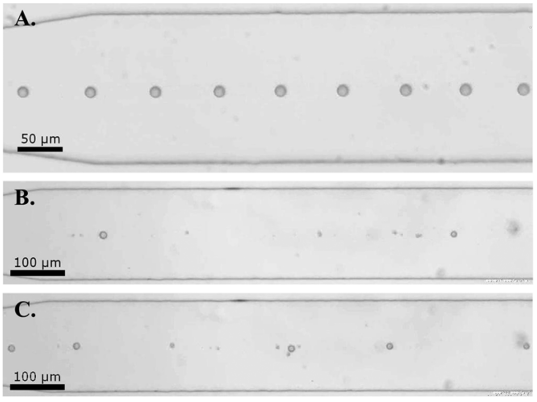

Figure 3. Droplet generation in the dripping regime within replicas produced from the original template. Frames taken from an image sequence recorded at 500 fps with an exposure time of 7 μs. (A) Continuous and stable generation of monodisperse droplets (10 μm diameter, 500 fL). Aqueous flow rate 59 nL/min, oil flow rate 899 nL/min. (B and C) Unstable generation of droplets (polydisperse, minimum 5 μm diameter, 70 fL). Aqueous flow rate <5 nL/min, oil flow rate ~1100 nL/min.

sizes down to 70 fL (5 μm diameter), but a stable and continuous production of monodisperse droplet sizes could not be maintained (Figure 3B and C; variability in the droplet diameter is observed in these video images).

Another mechanism has been described in the literature as the flow rate of oil is increased further, where a thin thread of the aqueous phase extends a long distance into the channel downstream of the four-way junction. The capillary breakup of the aqueous thread in the downstream channel can lead to variously sized droplets depending on the ratio of the flow rates of the oil and aqueous phases. At high ratios, the process is known as tip streaming, and small droplets ($\phi \leq 1$ μm) have been observed.[23,34,35] This is the most widely reported method for generating droplets in the femtoliter-volume range. However, the conditions for tip streaming are challenging to maintain for longer than transient time scales. Small fluctuations in the downstream flow conditions change the breakup distance, which leads to a dramatic change in the droplet size. Using the original template, flow conditions that led, even momentarily, to the formation and breakup of a thread of dispersed phase could not be found. A final regime for droplet formation at high capillary numbers is called jetting; this flow condition was also not observed in replicas from the original master. Hence, the smallest volume of aqueous droplets that could be produced reliably was 500 fL (corresponding to 10 μm diameter).

Since we could not identify conditions in which the replicas from the original template, with a 5 μm wide junction and a 15 μm channel height, would produce femtoliter droplets reliably, the effects of reducing the dimensions of the microfluidic component, as illustrated in Figure 4, were tested. In these experiments,

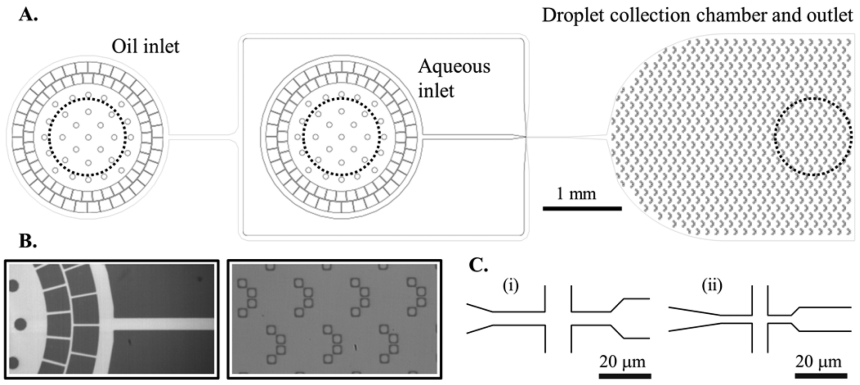

Figure 4. New template design. (A) Full pattern used to create the photomask (see description in the Experimental Methods). The dotted lines indicate the positions at which the tubing is inserted for delivery of oil and water and extraction of the mixed phase. (B) Cropped images of the new template illustrating a sample inlet with the internal filter and illustrating the droplet collection chamber including the pattern of square blocks that capture the aqueous droplets. (C) Enlarged view of the four-way junction in (i) the original template and (ii) the new template.

the surface tension of the aqueous phase was lowered by the addition of NP-40 (see Experimental Methods). Without the detergent, the maximum possible applied flow pressure was not sufficient to cause the water phase to enter the narrow 3 μm wide, 1.3 μm high junction at a sufficient flow rate for producing droplets with sizes equal to, or less than, the junction diameter by the dripping mechanism.

Different variants of the PFPE–PEG–PFPE triblock copolymer were tested in the oil phase, at a concentration of 3% m/v, to optimize the formation and stability of the aqueous droplets. The surfactant reduces the surface tension at the oil–water interface, which enables the aqueous droplets to be pinched off from the elongated flow and dispersed into the oil. The formation of large droplets by the squeezing mechanism was possible with a wide range of molecular masses for the PFPE (2500 to 7500 Da) and PEG (300 to 1000 Da) units. However, the generation of droplets with diameters of <10 μm without coalescence in the collection chamber was possible using the smallest molecular weight PFPE unit of 2500 Da in combination with PEG units of either 300, 400, 600, or 1000 Da and using the medium molecular weight PFPE unit of 3750 Da in combination with PEG units of either 600 or 1000 Da. The hydrophilic–lipophilic balance values for these fluorosurfactants ranged from 1.13 to 3.33. Similar fluorosurfactants have been reported in the literature for stabilizing larger droplets (>500 fL) by microfluidic flow focusing,[36,37] but they are normally prepared from Krytox 157FSH (7500 Da). The advantage of using the much smaller molecular weight PFPE unit of 2500 Da is that the fluorosurfactants are much easier to synthesize, characterize, and handle. Consequently, the results described in the remainder of this paper were obtained by adding the triblock copolymer, with 2500 Da for the PFPE unit and 300 Da for the PEG unit, to the oil phase.

The reduced dimensions for the four-way junction together with the optimized surfactant enabled the

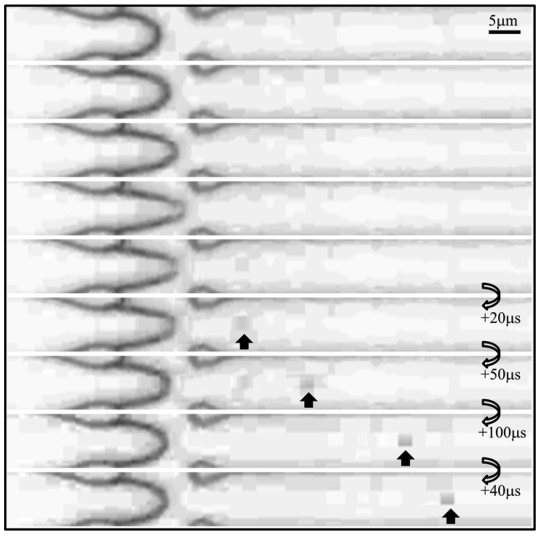

Figure 5. Droplet generation in the dripping regime within replicas produced from the new template. Image sequence recorded at 52 002 fps and 5 μs exposure time; frames shown at 0, 14.36, 16.71, 17.00, 17.08, 17.10, 17.15, 17.25, and 17.29 ms. Generation of one droplet with a diameter of approximately 1 μm. The dispersed phase protrudes into the four-way junction, where the downstream channel has an initial width of 3 μm, and the droplet is formed by the dripping mechanism. The generated droplet can be seen in the last three images as it moves in the downstream channel from left to right. The aqueous phase contains 0.5% NP-40.

controlled production of monodisperse droplets, with volumes of 1 to 5 fL, in a continuous stream under flow conditions that could be sustained for in excess of 10 min. Acquiring video images showing the formation of droplets with a volume of a few femtoliters was difficult due to the much higher velocity of the fluids in channels of lower cross sectional area. The formation of a single droplet occurred on a time scale of <1 ms. The video images shown in Figure 5 were obtained with an exposure time of 5 μs and a frame rate of 52002 fps, with an extremely low flow rate for the aqueous phase that led to long delays (approximately

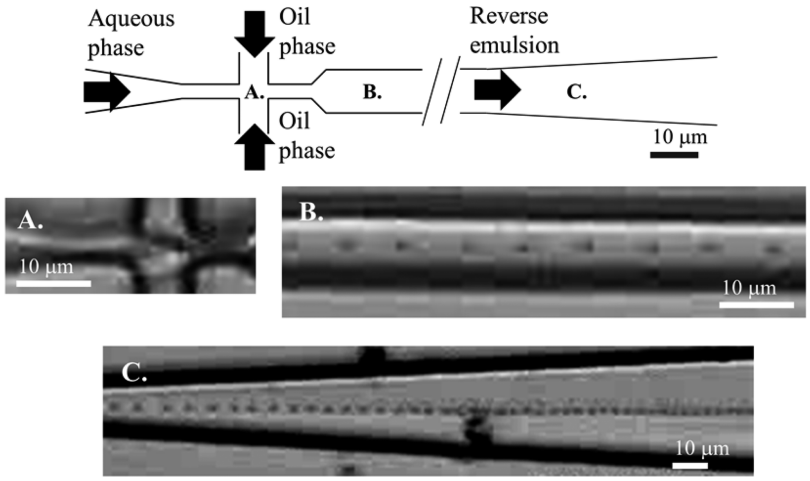

Figure 6. Droplet generation in replicas produced from the new template. Frames taken from an image sequence recorded with 47 μs exposure time. The formation of monodisperse droplets can be sustained for at least 10 min. (A) At higher flow rates, the dripping mechanism for droplet formation is maintained. (B) As the downstream channel widens, the droplet speed and the separation of droplets are reduced. (C) As the downstream channel widens further, the droplet separation begins to become nonuniform.

20 ms) between droplet formation events. The critical observation in this sequence of images is that the elongated flow of the aqueous phase protrudes into the four-way junction, where the droplet is pinched off from the pendant-shaped tip of the elongated flow. This is followed by the aqueous phase retreating back into the upstream microchannel, which is consistent with the dripping mechanism of droplet formation. The elongated flow of the aqueous phase does not extend into the single downstream channel, and the process of droplet formation does not rely on thread formation (*i.e.*, tip streaming), which is a flow condition that is difficult to sustain. The video images in Figure 5 show that the increase in pressure of the aqueous phase leads to only a subtle change in the position of the tip of the elongated flow.

In the example shown in Figure 5, the droplet will have traveled a substantial distance along the downstream channel before the formation of a subsequent droplet at the tip of the elongated flow can be observed. This contrasts with the relatively short spacing between the 500 fL droplets obtained using replicas made from the old template design. By increasing the flow rate for the aqueous phase, a higher density of droplets can be generated (see Figure 6). At these higher rates, the production of individual droplets could not be visualized in the video images. The images shown in Figure 6 of a stream of droplets, with sizes of approximately 1 fL (1 μm diameter), were obtained at low magnification in order to use shorter exposure times for sharper contrast. In this example, the faster flow rate for the aqueous phase does not appear to cause the mechanism for flow focusing to alter from dripping (see Figure 6A), and the elongated flow of the aqueous phase does not appear to enter the downstream channel during the formation of droplets. The size of the droplets remains approximately the same following the increase in the aqueous flow rate, and the rate of droplet production is more rapid. The speed of the femtoliter-sized droplets is reduced in the wider section of the downstream channel, and the separation between adjacent droplets is also reduced (Figure 6B and C). The flow conditions (*i.e.*, the relative pressures applied for delivery of oil and water) could be adjusted within a few seconds for the generation of femtoliter droplets (approximately 1 μm diameter), and a stable flow could be sustained in excess of 10 min.

A pressure-driven flow controller (Fluigent) was found to be indispensable for the formation of femtoliter droplet sizes; in contrast, suitable flow conditions could not be identified and maintained with syringe pumps. Droplets with spherical or ellipsoidal diameters between 1 and 3 μm could be generated by applying between 200 and 400 mbar pressure to the oil channel, with the aqueous channel pressure maintained at two-thirds of the pressure in the oil channel. Increasing the pressure ratio up to 3/4 resulted in ellipsoidal droplets of approximate diameter 3 to 4 μm, to 4/5 resulted in droplets of 4 to 5 μm in diameter, and 9/10 resulted in droplets of >5 μm in diameter. External measurement of flow rate could not be made accurately at the low values required to generate femtoliter droplets; however, an aqueous flow rate of approximately 10 nL/h and an oil flow rate of 300 nL/h were estimated from the frequency of droplet production in an image sequence recorded at 20 000 fps (47 μs exposure time) for the droplet train shown in Figure 6.

The femtoliter droplets are collected in a downstream chamber after production at the four-way junction by flow focusing. An outlet is located at the far end of the chamber. The microfluidic flow had to last for 1 min in order to yield a sufficient number of trapped droplets in the collection chamber. A bright-field image of droplets, with a mean ellipsoidal diameter

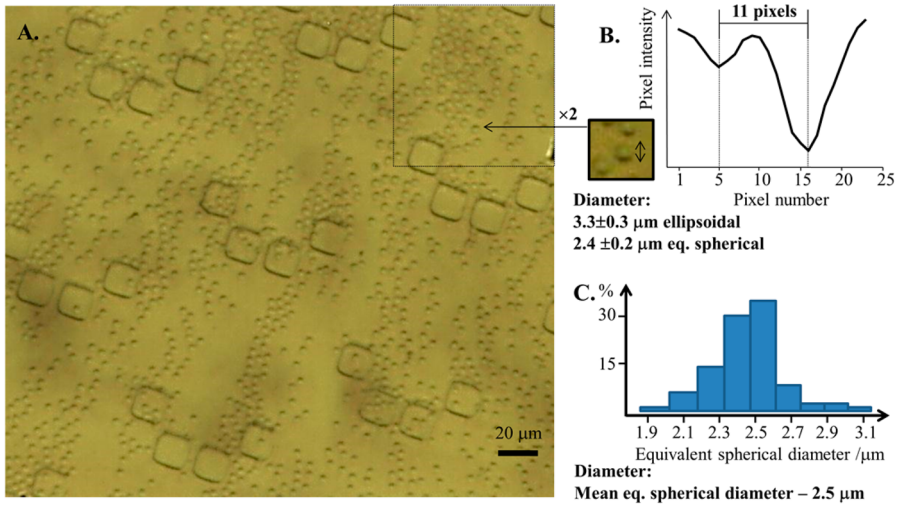

Figure 7. (A) Bright-field image of aqueous droplets in the collection chamber of the microfluidic device. The droplets are confined in a planar layer within the 1.3 μm channel height. (B) Diameter is estimated from the pixel-intensity profile of individual droplets, where the coordinates on the circumference of the droplet are determined that correspond to the longest vertical distance between intensity minima on the 2D image. (C) The histogram illustrates the sizes determined for 86 droplets in the region highlighted. The coordinate positions could not be identified for an additional 16 droplets in the same region. The mean ellipsoidal diameter is 3.4 μm (standard deviation 0.4 μm), with the axial dimension of the droplets restricted by the 1.3 μm channel height. The resulting equivalent mean spherical diameter of the droplets is 2.5 μm (8 fL volume).

of 3.4 μm (standard deviation of 0.4 μm), is shown in Figure 7A. The diameter is estimated for individual droplets from the pixel-intensity profile, where the coordinates on the circumference of the droplet are determined from the intensity minima on the longest vertical secant of the 2D image (see Figure 7B). The histogram shown in Figure 7C illustrates the sizes determined for 86 droplets in the region highlighted in Figure 7A; there were an additional 16 droplets in the same region for which the diameters could not be identified from the pixel-intensity profile. Droplets with a diameter that is larger than the height of the collection chamber (*i.e.*, 1.3 μm) will be ellipsoidal, rather than spherical, in shape. The mean ellipsoidal diameter of the measured droplets is 3.4 μm, and the resulting equivalent mean spherical diameter of the droplets is 2.5 μm (8 fL volume) in Figure 7A. The pressure-driven flow controller enabled the desired target diameters to be obtained within a few seconds, meaning that relatively small numbers of different-sized droplets were formed while the pressure values were adjusted. There is a small back flow of both aqueous and oil phases into the upstream channels when the flows are halted after 1 min. Conveniently, this prevents the inhomogeneously sized droplets produced at this stage from replacing the previously generated femtoliter droplets. The number of droplets trapped in the collection chamber of the microfluidic device is typically of the order of 10^4. The total viewing area of the collection chamber is approximately 6 mm^2, and the analyzed section shown in Figure 7A containing 102 droplets represents 7400 μm^2. Continued operation of the aqueous and oil flow leads to equal rates of population and loss of droplets from the collection chamber. Collected droplets do not show any signs of degradation over the course of 24 h storage at −5 °C.

Single-Molecule Fluorescence Imaging in Droplets of a Few Femtoliters. Transferring the microfluidic device containing the generated droplets to a fluorescence microscope enabled individual droplets to be analyzed under stationary conditions. Single droplets in the collection chamber were moved into the focus of the 488 nm laser beam by the translation of the microscope stage, and the fluorescence was recorded until the contents were photobleached by the excitation laser. The autofluorescence of the PDMS substrate is low and the emission from the encapsulated contents of a droplet can be easily discriminated from background light. As mentioned in the introduction, the design of the microfluidic device means that wide-field imaging of a large number of droplets would also be possible using either highly inclined thin illumination by a laser beam or total-internal-reflection fluorescence microscopy.

Quantum dots (QDot ITK 605 carboxyl, Invitrogen, Ltd.) were added initially to the aqueous phase and were encapsulated inside droplets on the microfluidic device. In these examples, the encapsulated volumes were larger than 1 fL so that the diffusional motion of the quantum dot in the droplet volume could be observed. In Figure 8A, the ellipsoidal droplets had a cross-sectional diameter of 4.5 μm (±0.5 μm) and the encapsulated volume would have been approximately 14 fL. The concentration of quantum dots was 8 nM in the aqueous phase (containing 0.5% m/v NP-40 and 0.1 M $MgCl_2$), giving an average of 66 quantum dots in each aqueous droplet. On the basis of the absence of any light emission from the surrounding oil phase, the

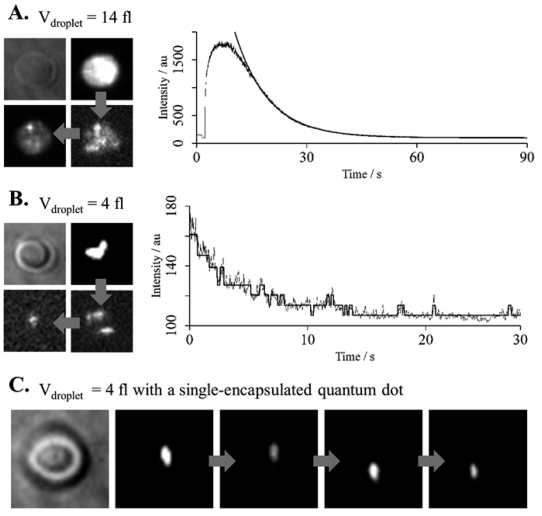

Figure 8. Photobleaching of droplet-confined quantum dots. (A) Images of 9 by 9 μm, recorded at 100 fps. Clockwise from top left of image sequence, the first image is an average over 150 frames recorded prior to illuminating the droplet with the laser; the second, third, and fourth images were taken after 7, 27, and 50 s, respectively. The integrated intensity−time trace is shown on the right. Following an initial period of photoactivation, the fluorescence intensity decays exponentially. (B) Images of 6.75 by 6.75 μm, recorded at 25 fps. Clockwise from top left of image sequence, the first image is an average over 35 frames recorded prior to illuminating the droplet with the laser; the second, third, and fourth images were taken after 0.08, 10.20, and 20.00 s. The integrated intensity−time trace is shown on the right. Seven bleaching steps are observed in the fluorescence intensity decay. (C) Images of 6.75 by 6.75 μm, recorded at 25 fps. Left to right of image sequence, the first image is an average over 30 frames recorded prior to illuminating the droplet with the laser; the second, third, fourth, and fifth images were recorded at intervals of 3 s.

quantum dots must have been confined to the dispersed phase and did not leak into the continuous phase. Intense emission was observed from the illuminated droplets (see Figure 8A). Initially, a subset of dark quantum dots in the droplet appears to undergo photoactivation by the laser radiation, and the cumulative emission intensity increases slowly. This process is counterbalanced by the photobleaching of bright quantum dots, which dominates after a short time, resulting in the exponential-like decay of emission intensity.

A lower concentration of quantum dots of 800 pM was used to obtain the data in Figure 8B. In this example, the ellipsoidal droplets were produced with a diameter of 2.5 μm ($\pm$0.5 μm). The encapsulated volume would have been approximately 4 fL, giving on average two quantum dots per droplet. Spatial fluctuations in the emission images, recorded by the EMCCD, are characteristic of the presence of discrete numbers of quantum dots in an isolated aqueous droplet. The intensity−time plots show a series of bleaching steps, and the number of quantum dots contained in a droplet could be estimated. Further reducing the concentration of quantum dots to 80 pM in the aqueous phase led to an average of 0.2 quantum dot encapsulated in a single droplet with an approximate diameter of 2.5 μm ($\pm$0.5 μm). In Figure 8C, an example of one of these droplets containing a single quantum dot is shown. The confined motion of a single quantum dot could be observed over time, and there was no apparent interaction between the quantum dot and the droplet interface.

In a second set of experiments, green-fluorescent protein (GFP) was added to the aqueous phase. In the first instance, a GFP concentration of 50 nM was used with 0.5% NP-40 and 0.1 M $MgCl_2$. Droplets were produced with a diameter of 3.0 μm ($\pm$0.5 μm), which would have been expected to encapsulate, on average, 180 molecules of GFP. A much smaller number was detected in these experiments; however, the origin of depletion of GFP levels was due to the protein adsorption on the surface of the plastic tubing delivering the aqueous solution to the microfluidic device rather than the transmission of GFP from aqueous droplets into the continuous oil phase on the microfluidic device. The fluorescence intensity of GFP is an order of magnitude less than the emission from a quantum dot, and the fluorescent protein bleaches at a faster rate. The detected fluorescence signal from a single, droplet-encapsulated, GFP molecule is just above the background signal observed from the fluorocarbon oil. Droplets containing multiple GFP molecules are uniformly bright with a clearly defined interface, which indicates that the GFP molecules are entirely confined to the aqueous droplets (see Figure 9A). Further evidence that the GFP molecules remained encapsulated inside the aqueous droplets was obtained by measuring different droplets before and after storage of the emulsion on the microfluidic device at −5 °C. In this case, the fluorescence-intensity levels were approximately the same for the droplet measured initially and the droplet measured following a period of 3 h of storage. A lower concentration of GFP of 5 nM was used to obtain the data in Figure 9B and C. Spatial fluctuations in the fluorescence images are observed for droplets containing smaller numbers of confined molecules, illustrating the free-diffusional motion of GFP.

The intensity−time plots shown in Figure 9 were background-signal corrected. Bleaching steps in the fluorescence intensity are observed in the background-corrected time plots (see Figure 9B and C), and it was possible to detect a single fluorescent protein encapsulated within an aqueous droplet; see Figure 9C, where the intensity−time plot shows a single photobleaching step.

DISCUSSION AND CONCLUSION

Although the use of microfluidic flow focusing to generate droplets of a suitable size for encapsulating single molecules has been reported before, there have been relatively few demonstrations of the suitability of this approach for single-molecule spectroscopy. Schaerli *et al.* have shown that picoliter droplets were

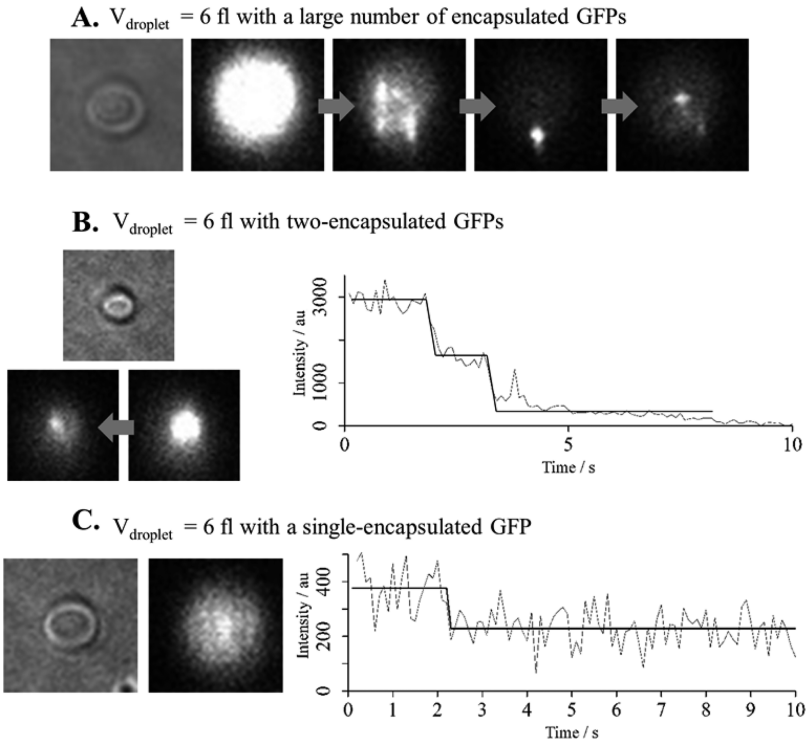

Figure 9. Photobleaching of droplet-confined green fluorescent protein. (A) Images of 8.4 by 8.4 μm, recorded at 10 fps. Left to right of image sequence, the first image is an average over 35 frames recorded prior to illuminating the droplet with the laser; the second, third, fourth, and fifth images were taken after 6.3, 8.4, 11.0, and 14.2 s, respectively. The fluorescent signal is confined to the droplet, and the gradual photobleaching of GFP molecules is observed. (B) Images of 8.4 by 8.4 μm, recorded at 10 fps. Clockwise from top left of image sequence, the first image is an average over 35 frames recorded prior to illuminating the droplet with the laser; the second and third images were taken after 0 and 2.7 s, respectively. The integrated intensity−time trace is shown on the right. Two bleaching steps are observed in the fluorescence intensity decay. (C) Images of 8.4 by 8.4 μm, recorded at 10 fps. The first image is an average over 41 frames recorded prior to illuminating the droplet with the laser; the second image was taken after 7.1 s. A single bleaching step can be seen. The integrated intensity−time trace is shown on the right. A single bleaching step is observed in the fluorescence intensity decay.

a suitable environment for polymerase chain reaction of single molecules of DNA,[38] and Courtois *et al*. were able to confine a single DNA molecular template in a picoliter volume for the *in vitro* expression and detection of a fluorescent protein.[39] Shim *et al*. observed, in recent work, the product turnover from single enzyme molecules in femtoliter droplets obtained by tip streaming in a flow-focusing device.[34] Many other examples of single-molecule enzymology[9−12] or PCR[30] in femtoliter droplets have been demonstrated. None of these earlier studies involve the detection of a single fluorescent molecule and, instead, the measurement is made from large numbers of fluorescent product molecules derived from enzyme-catalyzed reactions.

The present work takes advantage of the control and precision offered by flow focusing for the reliable production of monodisperse femtoliter droplets suitable for monitoring an encapsulated single fluorescent molecule. The fabricated devices generate aqueous femtoliter droplets by the dripping mechanism, rather than by thread formation in unstable flow regimes, and the dispersed phase remains in contact with the imaging surface for sensitive detection of fluorescence. In addition, the confinement of droplet flow to a two-dimensional plane will make it possible to use digital detection strategies in the future. It has been shown in the present work that single copies of green fluorescent protein can be encapsulated in femtoliter droplets and the stationary droplets can be monitored by fluorescence microscopy. Future applications of this method will result in the next generation of single-molecule experiments that avoid the preliminary step of tethering molecules to surfaces, which is essential for total-internal-reflection fluorescence microscopy, and enable the prolonged measurement on a molecule diffusing freely in solution.

EXPERIMENTAL METHODS

The original template was modified in a number of important respects to enable the production of smaller droplets (see Figure 4A), but the general layout of the features was not altered. The positions of the aqueous and oil inlets and the mixed-phase outlet are highlighted by the dotted lines. The circles located around the inlets and outlet acted as columns in the replicas to prevent sagging of the PDMS ceiling in shallow

microfluidic chambers. These features were present in the original template. The isosceles trapezia (Figure 4B) circulating the perimeter of the inlets acted as internal filters in the replicas to remove particles capable of blocking the narrow junction at the intersection of the aqueous and oil phases. Bifurcation of the oil channel, after the internal filter, provided a dual flow of fluid ahead of the four-way junction where the aqueous flow is focused into a single downstream channel. The height of the microfluidic channels was reduced from 15 μm in the original template to 1.3 μm in the new template. The separation between the filter blocks (trapezia in Figure 4B) was reduced from 11 μm to 8 μm in the inner circle and from 8 μm to 5 μm in the outer circle. The initial width of both the aqueous and oil channels was reduced from 170 μm to 60 μm. The width of the aqueous channel along the tapered section that extends through the junction was reduced from 5 μm to 3 μm. The tapered section of the oil channels leading to the junction was also reduced from 15 μm to 9 μm. The channel downstream of the junction contained the mixed flow of the immiscible phases. In the original template, it expanded to a width of 165 μm (see Figure 4C) and was directed straight toward the outlet. In the new template, it expanded to a 60 μm width and led into a droplet collection chamber (Figure 4A). The repeated pattern of squares, with sides of 20 μm (see Figure 4B), located inside this chamber had a dual function. First, they acted as columns to prevent sagging of the PDMS ceiling. Second, the square-based columns were arranged appropriately, in groups of four, to spread the flow of the water-in-oil emulsion and capture the aqueous droplets ahead of the outlet in the microfluidic component. This enables the spectroscopic analysis of the aqueous droplets on-board the microfluidic component.

Fabricating a New Master Template for Microfluidic Components. A negative image of a large number of copies of the microfluidic design shown in Figure 4A was drawn in Adobe Illustrator software (Adobe Systems) and converted to a Gerber file format. The image was reproduced at 128 00 dpi on a chrome layer supported on 0.060 in. thick soda lime (JD Photo-Tools). Boron-doped silicon (100) wafers, with a diameter of 2 in. and a thickness of 280 μm (1−10 Ω·cm), were used as substrates to manufacture the master template (MicroChemical GmbH). A permanent epoxy negative photoresist (SU-8 2002, MicroChem Corp.) was spin coated (500 rpm, 30 s, followed by 1500 rpm, 30 s) onto the polished silicon surface to produce a uniform layer of 1.3 μm thickness, which was cured by a soft bake at 95 °C for 1 min. Coated silicon wafers were clamped on a vacuum chuck in a home-built photolithography apparatus. A vertical linear stage brought the photoresist-coated surface of the wafer into contact with the photomask, and uniform UV illumination of 550−650 mJ cm^{-2} (incident on the photomask), across the 2 in. diameter area, was provided by a commercial 365 nm LED curing lamp (DELOLUX 80/365, Delo Industrial Adhesives). Following a postbake at 95 °C for 6 min, the photoresist was developed in Microposit EC solvent (MicroChem Corp.) and cleaned with acetone. The template was fabricated in filtered air within a horizontal laminar flow hood.

An optical profilometer (Zeta-20, Zeta Instruments) was used to check the three-dimensional surface pattern on the silicon wafers. The smallest feature size of the microfluidic design is the width of the four-way junction, and the 3D profile of the junction in a photoresist layer on a silicon wafer is shown in Figure 10. The junction is reproduced precisely with a height of 1.3 μm and a width of 3.1 μm.

Producing Replicas of the Microfluidic Components in PDMS. Replicas of the new template in Figure 4A were produced in polydimethylsiloxane. The base and hardener components of the silicone adhesive were mixed in a ratio of approximately 10:1 and cast over the patterned surface on the silicon wafer in a disposable plastic Petri dish. The thickness of the adhesive layer was approximately 5 mm. The PDMS was degassed in a vacuum desiccator prior to precuring at 65 °C for 2 h, with postcuring overnight at room temperature. The outline of a rectangle (approximately 25 by 35 mm) surrounding 12 copies of the microfluidic design was cut into the cured PDMS, and the enclosed segment was separated from the silicon wafer. A 0.7 mm biopsy punch was used to bore holes at the positions indicated by the dotted circles in Figure 4A on the patterns transferred to the PDMS. After the microfluidic component was assembled, the connections to the inlet and outlet channels were made by inserting 0.042 in. o.d. tubing (Microbore PTFE tubing, Cole-Parmer) into the bored holes. The PDMS surface and a #1 cover glass (Menzel-Gläser, 24 mm by 50 mm) were activated with an oxygen plasma for 1 min at 0.1 mbar and 28 W (MiniFlecto-PC-MFC, Gala Instrumente). The cover glass was then pressed firmly against the patterned surface of the PDMS to seal the channels for the microfluidic components and placed in an oven at 65 °C for 1 h.

An additional step was required for producing replicas of the new template with a channel height of 1.3 μm. The reduced thickness of the photoresist layer means that the aspect ratio was high for the aqueous and oil channels downstream of the four-way junction (the ratio of width to height is approximately 40). In these regions, the sagging of the PDMS ceiling would normally block the channels and restrict fluid flow; this is illustrated by the reduced contrast in the wider sections of the microfluidic channels for a PDMS replica in Figure 11. The maximum aspect ratio for which the collapse of microfluidic channels can be avoided is widely regarded to be ~20, and this requires the use of a larger proportion of hardener in the precured PDMS mixture (a base-to-hardener ratio of 7:1 increases significantly the stiffness of the polymer).[40] It was not practical to reduce the width of the channels throughout the microfluidic design in order to maintain an aspect ratio of <20 because the high pressure required for pushing the aqueous and oil phases through the channels would cause the PDMS to delaminate from the cover glass. Avoiding the collapse of microfluidic channels in regions of high aspect ratio was achieved by covering the patterned PDMS surface in methanol (HPLC grade), prior to sealing the channels against the cover glass. The methanol layer prevented the surfaces from bonding instantaneously when brought into contact. The solvent evaporated in the oven at 65 °C, allowing the PDMS to bond to the cover glass in the absence of an external compressive force.[41]

The microfluidic replicas produced from the original template, containing wider and deeper channels, were flushed with a 1% solution of 3-aminopropyltriethoxysilane in FC-40 (Fluorinert, 3M) and left overnight. Both the PDMS and glass

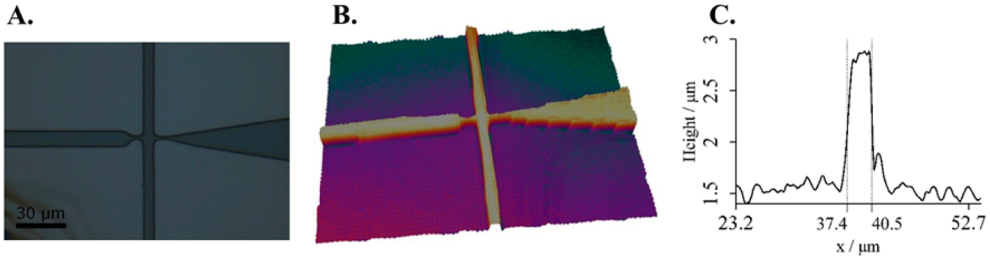

Figure 10. Four-way junction in the new template design. (A) Image of the photoresist layer on the silicon wafer. (B) Surface profile of the photoresist layer on the silicon wafer. (C) The smallest dimension of 3 μm rendered on the UV photomask is accurately transferred to the photoresist layer (this is located in the exit channel immediately following the four-way junction). The thickness of the photoresist layer was 1.3 μm.

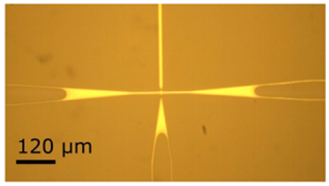

Figure 11. PDMS replica from the new template design in which the microfluidic channels are sealed onto a microscope cover glass. The darker regions indicate where the ceiling of the microfluidic channels have collapsed due to the large aspect ratio of the channel dimensions. Bonding with methanol as a separating layer prevented the collapse of the channel ceiling.

surfaces are hydrophilic following plasma treatment, and water will tend to become the continuous phase in flow focusing under these conditions. The contact angle of pure water on untreated and plasma-treated glass is approximately 67° and <5°, respectively, and that on untreated and plasma-treated PDMS is approximately 91° and 12°, respectively. The effect of the silanizing agent was to reduce the hydrophilic property of the channels while still maintaining a sufficiently low interfacial tension between the aqueous phase and the surfaces to facilitate the pressure-driven flow. The contact angle of water on glass and PDMS following treatment with the silanizing agent is 20° and 19°, respectively. This pretreatment was not performed for the microfluidic replicas produced from the new template containing features of 1.3 μm height. In the shallow microchannels, the increase in the interfacial tension caused by addition of the silanizing agent restricted the flow of the aqueous phase, and it was critical that the highly hydrophilic surfaces produced by plasma treatment were retained. It was also necessary to further reduce the interfacial tension by addition of the detergent, 0.5% m/v Tergitol-type NP-40 (nonyl phenoxypolyethoxylethanol). Unlike the example of the replicas from the original template, it was found that the plasma-treated surfaces for replicas from the new template design did not result in the dispersion of oil in a continuous phase of water.

Pressure-Driven Flow of Aqueous and Oil Phases and Formation of Aqueous Microdroplets. Custom triblock copolymers were synthesized from perfluoropolyether carboxylic acids (PFPE, 2500 to 7500 $g \cdot mol^{-1}$) and polyethylene glycol (PEG, 300 to 1000 $g \cdot mol^{-1}$). The product, PFPE–PEG–PFPE, is a nonionic surfactant with ester linkages between the PFPE and PEG components. Similar surfactants have been described by others.[36,42,43] Krytox 157FSL, 157FSM, and 157FSH were obtained from Dupont and were used as supplied. Perfluorohexane was purchased from Fluorochem Ltd. and dried by refluxing over calcium hydride. The polyethylene glycols (300, 400, 600, and 1000 Da) were purchased from Sigma-Aldrich. Each of the polyethylene glycols were dissolved in toluene, distilled to remove any trace water, and then dried *in vacuo* at 110 °C for 4 h. The triblock copolymers PFPE–PEG–PFPE were synthesized using a method modified from the literature.[37] The perfluoropolyether carboxylic acids were refluxed with 10 equiv of oxalyl chloride in dry perfluorohexane for 24 h under an atmosphere of nitrogen. After cooling the reaction mixture to room temperature, the perfluorohexane and the excess oxalyl chloride were removed on a Schlenk line to give the perfluoropolyether acid chloride as a clear oil, which was stored under nitrogen. Two equivalents of the perfluoropolyether acid chloride were then reacted with 1 equiv of the dry polyethylene glycol in the presence of dry pyridine in a solvent mixture of dry benzotrifluoride and dry perfluorohexane. The reaction mixture was refluxed under a nitrogen atmosphere for 24 to 72 h. After cooling to room temperature, the reaction mixture was filtered and the excess solvent was removed using a rotary evaporator. The crude product was dissolved in perfluorohexane and was washed with water. The organic layer was dried over $MgSO_4$ and $CaCl_2$ and filtered, and the solvent was removed to give the fluorosurfactant as a clear oil.

The PEG component in the triblock copolymer provides an inert biocompatible surface in the interior of the aqueous droplet. The surfactant (3% to 6% m/v) was added to the oil phase, FC-40. Both the aqueous and oil phases were delivered to a microfluidic component by a pressure-driven flow controller (MFCS, Fluigent). The pressure applied to the aqueous and oil phases can be manipulated separately to enable the droplet size to be adjusted. Flow conditions respond immediately following adjustment of pressures. Typical flow rates applied were in the region of 10 nL/h for the aqueous phase and 300 nL/h for the oil phase to observe the formation of femtoliter droplets. The formation of droplets at the junction between the aqueous and oil flows was visualized using a 5× objective lens (MPlan Apo, Mitoyo) with a zoom lens (0.7× to 4.5×, Zoom 6000, Navitar Inc.) and a 2× magnification camera adapter. The overall magnification could be varied from 7× to 45× on an imaging detector with a 5.5 μm pixel size (Basler Ace acA2000-340kc). Bright-field images were also collected with a high frame rate camera (>20k fps, MotionXtra NX-4S3, IDT Ltd.).

The internal volume of the PTFE tubing between the sample vial on the flow controller and the microfluidic component was approximately 50 μL. Accordingly, the minimum volume of the aqueous sample required in an experiment to generate a stream of microdroplets was 100 μL. If necessary, a smaller volume of sample could be used by injecting the aqueous phase (1 to 20 μL) into a flow of the FC-40 oil using a high-performance liquid chromatography sample-inlet valve (Rheodyne model 7125 syringe loading injector). In this case, the aqueous phase traveled as a plug in the oil flow along the PTFE tubing and into the aqueous inlet of the microfluidic component. The aqueous plug flowed along the central channel, leading to the four-way junction, where it was dispersed into a short stream of droplets. In this mode of operation, the internal filter for the aqueous inlet channel must be eliminated, as otherwise it would lead to the upstream breakup of the aqueous plug.

Single-Molecule Fluorescence Microscopy of Droplets. Fluorescence measurements on the microdroplets trapped in the upstream collection chamber were made on a home-built inverted microscope with a 100 × /1.25NA oil immersion objective lens. The back aperture of the objective lens was overfilled with the collimated beam of a 488 nm laser. The diffraction-limited beam waist of the laser was positioned on an aqueous microdroplet. The fluorescence light was collected by the objective lens, separated from the laser light by a dichroic mirror (and a 488 nm notch filter), and imaged onto an electron-multiplied charge-coupled device (iXon DU867, Andor). The acquired data were saved in Tagged Image File Format, and single images and intensity–time plots were obtained using the open source image processing software Fiji. Background-corrected intensity–time plots were calculated by determining the mean pixel intensity from an area twice as large as that occupied by a single aqueous droplet. Reversible and irreversible changes of the fluorescence intensity due to either variations in quantum yield or the bleaching of fluorophores were analyzed. In the latter case, the assignment and counting of bleaching steps enabled the determination of the number of fluorescent proteins present in an aqueous droplet.

Bleaching steps were identified with a custom-written algorithm that employs a Bayesian method to determine the likelihood of a step change in the fluorescence intensity.[44] If the likelihood exceeds the set threshold, the intensity–time plot is divided at this point into subplots and the algorithm searches for the next occurrence of a step change. The procedure is repeated until either there are no further step changes in intensity or the remaining length of a subplot is too short to identify a step change with sufficient certainty. The exact time points for step changes are further refined; they need to be separated by at least three data points, and the resulting step height has to be above the mean noise level to prevent a false positive originating from the inherent signal fluctuations.

Conflict of Interest: The authors declare no competing financial interest.

Acknowledgment. We would like to thank Prof. Andrew Griffiths (ParisTech) for providing a master template to produce the original microfluidic replicas and Dr. Jon Howell (DuPont Chemicals and Fluoroproducts) for the kind donation of Krytox

157FSL, 157FSM, and 157FSH, which were used to synthesise a range of fluorosurfactants. We would also like to thank Dr. Julie Pratt for helpful discussions.

REFERENCES AND NOTES

1. Hodson, M. J.; Hudson, A. J.; Cherny, D.; Eperon, I. C. The Transition in Spliceosome Assembly from Complex E to Complex A Purges Surplus U1 snRNPs from Alternative Splice Sites. *Nucleic Acids Res.* **2012**, *40*, 1–13.
2. Cherny, D.; Gooding, C.; Eperon, G. E.; Coelho, M. B.; Bagshaw, C. R.; Smith, C. W. J.; Eperon, I. C. Stoichiometry of a Regulatory Splicing Complex Revealed by Single-Molecule Analyses. *EMBO J.* **2010**, *29*, 2161–2172.
3. Tokunaga, M.; Imamoto, N.; Sakata-Sogawa, K. Highly Inclined Thin Illumination Enables Clear Single-Molecule Imaging in Cells. *Nat. Methods* **2008**, *5*, 159–161.
4. Ishitsuka, Y.; Okumus, B.; Arslan, S.; Chen, K. H.; Ha, T. Temperature-Independent Porous Nanocontainers for Single-Molecule Fluorescence Studies. *Anal. Chem.* **2010**, *82*, 9694–9701.
5. Boukobza, E.; Sonnenfeld, A.; Haran, G. Immobilization in Surface-Tethered Lipid Vesicles as a New Tool for Single Biomolecule Spectroscopy. *J. Phys. Chem. B* **2001**, *105*, 12165–12170.
6. Tawfik, D. S.; Griffiths, A. D. Man-Made Cell-like Compartments for Molecular Evolution. *Nat. Biotechnol.* **1998**, *16*, 652–656.
7. Reiner, J. E.; Crawford, A. M.; Kishore, R. B.; Goldner, L. S.; Helmerson, K.; Gilson, M. K. Optically Trapped Aqueous Droplets for Single Molecule Studies. *Appl. Phys. Lett.* **2006**, *89*, 013904.
8. Tang, J.; Jofre, A. M.; Kishore, R. B.; Reiner, J. E.; Greene, M. E.; Lowman, G. M.; Denker, J. S.; Willis, C. C. C.; Helmerson, K.; Goldner, L. S. Generation and Mixing of Subfemtoliter Aqueous Droplets on Demand. *Anal. Chem.* **2009**, *81*, 8041–8047.
9. Rondelez, Y.; Tresset, G.; Tabata, K. V.; Arata, H.; Fujita, H.; Takeuchi, S.; Noji, H. Microfabricated arrays of femtoliter chambers allow single molecule enzymology. *Nat. Biotechnol.* **2005**, *23*, 361–365.
10. Iino, R.; Hayama, K.; Amezawa, H.; Sakakihara, S.; Kim, S. H.; Matsumono, Y.; Nishino, K.; Yamaguchi, A.; Noji, H. A single-cell drug efflux assay in bacteria by using a directly accessible femtolitre droplet array. *Lab Chip* **2012**, *12*, 3923–3929.
11. Ota, S.; Kitagawa, H.; Takeuchi, S. Generation of Femtolitre Reactor Arrays within a Microfluidic Channel for Biochemical Analysis. *Anal. Chem.* **2012**, *84*, 6346–6350.
12. Witters, D.; Knez, K.; Ceyssens, F.; Puers, R.; Lammertyn, J. Digital microfluidics-enabled single-molecule detection by printing and sealing single magnetic beads in femtolitre droplets. *Lab Chip* **2013**, *13*, 2047–2054.
13. Wu, T.; Hirata, K.; Suzuki, H.; Xiang, R.; Tang, Z.; Yomo, T. Shrunk to femtolitre: Tuning high-throughput monodisperse water-in-oil droplet arrays for ultra-small microreactors. *Appl. Phys. Lett.* **2012**, *101*, 074108.
14. Anna, S. L.; Bontoux, N.; Stone, H. A. Formation of Dispersions Using "flow Focusing" in Microchannels. *Appl. Phys. Lett.* **2003**, *82*, 364.
15. Huebner, A.; Sharma, S.; Srisa-Art, M.; Hollfelder, F.; Edel, J. B.; Demello, A. J. Microdroplets: A Sea of Applications? *Lab Chip* **2008**, *8*, 1244–1254.
16. Theberge, A. B.; Courtois, F.; Schaerli, Y.; Fischlechner, M.; Abell, C.; Hollfelder, F.; Huck, W. T. S. Microdroplets in Microfluidics: An Evolving Platform for Discoveries in Chemistry and Biology. *Angew. Chem., Int. Ed.* **2010**, *49*, 5846–5868.
17. Teh, S.-Y.; Lin, R.; Hung, L.-H.; Lee, A. P. Droplet Microfluidics. *Lab Chip* **2008**, *8*, 198–220.
18. Guo, M. T.; Rotem, A.; Heyman, J. A.; Weitz, D. A. Droplet Microfluidics for High-Throughput Biological Assays. *Lab Chip* **2012**, *12*, 2146–2155.
19. Taly, V.; Kelly, B. T.; Griffiths, A. D. Droplets as Microreactors for High-Throughput Biology. *ChemBioChem* **2007**, *8*, 263–272.
20. Dittrich, P. S.; Jahnz, M.; Schwille, P. A New Embedded Process for Compartmentalized Cell-Free Protein Expression and on-Line Detection in Microfluidic Devices. *ChemBioChem* **2005**, *6*, 811–814.
21. Xu, S.; Nie, Z.; Seo, M.; Lewis, P.; Kumacheva, E.; Stone, H. A.; Garstecki, P.; Weibel, D. B.; Gitlin, I.; Whitesides, G. M. Generation of Monodisperse Particles by Using Microfluidics: Control over Size, Shape, and Composition. *Angew. Chem.* **2005**, *117*, 734–738.
22. Lee, W.; Walker, L. M.; Anna, S. L. Role of Geometry and Fluid Properties in Droplet and Thread Formation Processes in Planar Flow Focusing. *Phys. Fluids* **2009**, *21*, 032103.
23. Anna, S. L.; Mayer, H. C. Microscale Tipstreaming in a Microfluidic Flow Focusing Device. *Phys. Fluids* **2006**, *18*, 121512.
24. Shui, L.; van den Berg, A.; Eijkel, J. C. T. Scalable attolitre monodisperse droplet formation using multiphase nanomicrofluidics. *Microfluid. Nanofluid.* **2011**, *11*, 87–92.
25. Arayanarakool, R.; Shui, L.; Kengen, S. W. M.; van den Berg, A.; Eijkel, J. C. T. Single-enzyme analysis in a droplet-based micro- and nanofluidic system. *Lab Chip* **2013**, *13*, 1955–1962.
26. Yang, Y.-J.; Feng, X.; Xu, N.; Pang, D.-W.; Zhang, Z.-L. Generation of sub-femtolitre droplet by T-junction splitting on microfluidic chips. *Appl. Phys. Lett.* **2013**, *102*, 123502.
27. Kobayashi, I.; Mukataka, S.; Nakajima, N. Production of Monodisperse Oil-in-Water Emulsions Using a Large Silicon Straight-Through Microchannel Plate. *Ind. Eng. Chem. Res.* **2005**, *44*, 5852–5856.
28. Couture, O.; Faivre, M.; Pannacci, N.; Babataheri, A.; Servois, V.; Tabeling, P.; Tanter, M. Ultrasound internal tattooing. *Med. Phys.* **2011**, *38*, 1116–1123.
29. Cohen, C.; Giles, R.; Sergeyeva, V.; Mittal, N.; Tabeling, P.; Zerrouki, D.; Baudry, J.; Bibette, J.; Bremond, N. Parallelised production of fine and calibrated emulsions by coupling flow-focussing and partial wetting phenomenon. *Microfluid. Nanofluid.* **2014**, *17*, 959–966.
30. Leman, M.; Abouakil, F.; Griffiths, A. D.; Tabeling, P. Droplet-based microfluidics at the femtolitre scale. *Lab Chip* **2015**, *15*, 753–765.
31. Prof. Andrew Griffiths, Laboratoire de Biochimie, Building B, ESPCI ParisTech, 10 Rue Vauquelin, 75005 Paris, France.
32. Garstecki, P.; Stone, H. A.; Whitesides, G. M. Mechanism for Flow-Rate Controlled Breakup in Confined Geometries: A Route to Monodisperse Emulsions. *Phys. Rev. Lett.* **2005**, *94*, 164501.
33. Garstecki, P.; Fuerstman, M. J.; Stone, H. A.; Whitesides, G. M. Formation of droplets and bubbles in a microfluidic T-junction - scaling and mechanism of break-up. *Lab Chip* **2006**, *6*, 437–446.
34. Shim, J.; Ranasinghe, R. T.; Smith, C. A.; Ibrahim, S. M.; Hollfelder, F.; Huck, W. T.; Klenerman, D.; Abell, C. Ultrarapid Generation of Femtoliter Microfluidic Droplets for Single-Molecule-Counting Immunoassays. *ACS Nano* **2013**, *7*, 5955–5964.
35. Ward, T.; Faivre, M.; Stone, H. A. Drop Production and Tip-Streaming Phenomenon in a Microfluidic Flow-Focusing Device via an Interfacial Chemical Reaction. *Langmuir* **2010**, *26*, 9233–9239.
36. Holtze, C.; Rowat, A. C.; Agresti, J. J.; Hutchison, J. B.; Angilè, F. E.; Schmitz, C. H. J.; Köster, S.; Duan, H.; Humphry, K. J.; Scanga, R. A.; et al. Biocompatible Surfactants for Water-in-Fluorocarbon Emulsions. *Lab Chip* **2008**, *8*, 1632–1639.
37. Chen, F.; Zhan, Y.; Geng, T.; Lian, H.; Xu, P.; Lu, C. Chemical Transfection of Cells in Picoliter Aqueous Droplets in Fluorocarbon Oil. *Anal. Chem.* **2011**, *83*, 8816–8820.
38. Schaerli, Y.; Wootton, R. C.; Robinson, T.; Stein, V.; Dunsby, C.; Neil, M. A. A.; French, P. M. W.; Demello, A. J.; Abell, C.; Hollfelder, F. Continuous-Flow Polymerase Chain Reaction of Single-Copy DNA in Microfluidic Microdroplets. *Anal. Chem.* **2009**, *81*, 302–306.
39. Courtois, F.; Olguin, L. F.; Whyte, G.; Bratton, D.; Huck, W. T. S.; Abell, C.; Hollfelder, F. An Integrated Device for

Monitoring Time-Dependent in Vitro Expression from Single Genes in Picolitre Droplets. *ChemBioChem* **2008**, *9*, 439–446.
40. Xia, Y.; Whitesides, G. Soft Lithography. *Annu. Rev. Mater. Sci.* **1998**, *28*, 153–185.
41. Orabona, E. *Microfluidics Assisted Platforms for Biotechnological Applications*; Università di Napoli Federico II, 2011.
42. Holt, D. J.; Payne, R. J.; Abell, C. Synthesis of Novel Fluorous Surfactants for Microdroplet Stabilisation in Fluorous Oil Streams. *J. Fluorine Chem.* **2010**, *131*, 398–407.
43. Chiu, Y.-L.; Chan, H. F.; Phua, K. K. L.; Zhang, Y.; Juul, S.; Knudsen, B. R.; Ho, Y.-P.; Leong, K. W. Synthesis of Fluorosurfactants for Emulsion-Based Biological Applications. *ACS Nano* **2014**, *8*, 3913–20.
44. Ruanaidh, O.; Joseph, J. K.; Fitzgerald, W. J. *Numerical Bayesian Methods Applied to Signal Processing*; Springer: New York, 1996.